Quantitative Conformational Measurements in Solid State NMR by Constant-Time Homonuclear Dipolar Recoupling

Andrew E. Bennett, David P. Weliky, and Robert Tycko*

Laboratory of Chemical Physics, National Institute of Diabetes and Digestive and Kidney Diseases National Institutes of Health Bethesda, Maryland 20892-0520

Received January 20, 1998

Solid-state nuclear magnetic resonance (NMR) techniques provide structural information at atomic-level detail in complex, disordered, molecular solids. Structural information from solid-state NMR measurements takes the form of internuclear distances,[1−3] dihedral or other angles,[4,5] or orientations of chemical groups,[6] depending on the techniques employed and the nature of the sample. Information about internuclear distances and dihedral angles can be obtained from measurements of magnetic dipole−dipole couplings between isotopically labeled nuclei carried out with magic-angle spinning (MAS) and dipolar recoupling techniques.[1−3,5] Typically, recoupling techniques yield dipolar evolution curves that are analyzed by comparison with simulations of nuclear spin dynamics[1,2,5] or with numerical expressions.[3] The precision and accuracy of dipolar recoupling techniques are often limited by difficulties in measuring such dipolar evolution curves without damping or distortion from effects that cannot be simulated accurately. This is particularly true of homonuclear recoupling techniques (e.g., measurements of $^{13}C-^{13}C$ or $^{15}N-^{15}N$ couplings), where several factors can distort dipolar evolution curves and prevent quantitative comparisons of experimental and simulated data: (1) radio frequency (rf) pulse sequences designed to average out chemical shift differences and chemical shift anisotropies (CSA) may not do so adequately, especially in high fields; (2) significant rf inhomogeneity may be present, particularly in measurements on biomolecular systems where sensitivity considerations prohibit the use of small sample volumes; (3) residual couplings to protons may be significant even under high-power decoupling, due to the difficulty of decoupling protons during a dense rf pulse train on the nuclei of interest; (4) transverse relaxation processes may be important. These factors become increasingly important as the internuclear distances become larger and the dipolar evolution periods become correspondingly longer.

Here we describe an approach to homonuclear dipolar recoupling in solid-state NMR that addresses the above experimental problems. We have developed this approach for studies of peptide backbone conformations, carried out on peptides with ^{13}C labels at two successive backbone carbonyl sites, but the approach is applicable to any similar problem in which the CSA tensors of the labeled sites are well characterized. The elements of the approach are as follows: (1) We use the "rf-driven recoupling" (RFDR) sequence[1] to generate a nonzero average dipole−dipole coupling under MAS. RFDR has the advantages of being effective when the CSA is large, insensitive to inhomogeneous broadening of the NMR lines, and extremely sparse, so that effects of pulse imperfections and signal losses due to insufficient proton decoupling are minimized. With XY-32 cycling of the π pulses in the RFDR train,[7] the sequence is insensitive to rf inhomogeneities up to roughly ±10%. The average dipole−dipole coupling Hamiltonian under RFDR has the form $\tilde{H}_{dd} = d(I_{1+}I_{2-} + I_{1-}I_{2+})$, where I_{i+} is the angular momentum raising operator for spin i and d is the effective coupling constant.[1] (2) We incorporate RFDR into a double-quantum filtering sequence.[8] Double-quantum filtering selects signals from coupled pairs of ^{13}C nuclei, strongly attenuating natural-abundance signals that would otherwise partially mask the signals of interest in systems of high molecular weight. The basic sequence for double-quantum filtering has the form $CP_{90+\zeta}-(RFDR)_L-90_\zeta-90_0-(RFDR)_M-$FID, where CP represents cross-polarization from protons to ^{13}C nuclei, 90_ζ represents a $\pi/2$ pulse with rf phase ζ, $(RFDR)_L$ represents an RFDR train lasting L MAS rotor periods τ_R, and FID represents the detection of free-induction-decay signals. FIDs are recorded with $\zeta = 0°$, 90°, 180°, and 270° and coadded after multiplication by $e^{2i\zeta}$. (3) We implement *constant-time* versions of double-quantum filtering by extending the sequence to $CP_{90+\zeta}-(RFDR)_L-90_\zeta-90_0-(RFDR)_M-90_{180}-90_{90}-(RFDR)_N-$FID. For a pair of spin-1/2 nuclei with coupling $\tilde{H}_{dd}$, the second pair of $\pi/2$ pulses can be shown to refocus dipolar evolution, in analogy to a Hahn spin−echo. In an ideal system, NMR signals from the extended sequence would therefore be the same as signals from the sequence $CP_{90+\zeta}-(RFDR)_L-90_\zeta-90_0-(RFDR)_{M-N}-$FID. In a real system, the extended sequence allows the total recoupling period $T = (L + M + N)\tau_R$ to be kept constant throughout an experiment while the effective dipolar evolution periods are varied by varying L, M, and N. The coupled two-spin system contains only single-quantum coherences during evolution under RFDR, except during the π pulses themselves. Residual carbon−proton couplings and transverse relaxation processes are therefore expected to have little effect on the dipolar evolution curves.

Figure 1 shows two examples of constant-time double-quantum-filtered dipolar evolution curves for a doubly^{13}C-labeled powder sample of the tripeptide alanylglycylglycine (AGG). Figure 1a is a "constant-time double-quantum build-up" (CTDQBU) curve, obtained by incrementing L from 0 to L_{max}, setting $M = L_{max}$, and setting $N = L_{max} - L$. Figure 1b is a "constant-time double-quantum-filtered dipolar dephasing" (CTDQFD) curve, obtained by setting L to a constant value L_0, incrementing M from $M_{max}/2$ to M_{max}, and setting $N = M_{max} - M$. For both curves, a least-squares fit of experimental data to simulations is shown, with the only adjustable parameter being the overall scaling of the

(1) (a) Bennett, A. E.; Griffin, R. G.; Vega, S. *NMR Basic Prin. Prog.* **1994**, *33*, 1−77. (b) Bennett, A. E.; Ok, J. H.; Vega, S.; Griffin, R. G. *J. Chem. Phys.* **1992**, *96*, 8624−8627. (c) Gullion, T.; Vega, S. *Chem. Phys. Lett.* **1992**, *194*, 423−428.

(2) (a) Tycko, R.; Dabbagh, G. *Chem. Phys. Lett.* **1990**, *173*, 461−465. (b) Levitt, M. H.; Raleigh, D. P.; Creuzet, F.; Griffin, R. G. *J. Chem. Phys.* **1990**, *92*, 6347−6364. (c) Gregory, D. M.; Mitchell, D.; Stringer, J. A.; Kiihne, S. R.; Shiels, J. C.; Callahan, J.; Mehta, M. A.; Drobny, G. P. *Chem. Phys. Lett.* **1995**, *246*, 654−663. (d) Lee, Y. K.; Kurur, N. D.; Helmle, M.; Johannessen, O. G.; Nielsen, N. C.; Levitt, M. H. *Chem. Phys. Lett.* **1995**, *242*, 304−309. (e) Fujiwara, T.; Ramamoorthy, A.; Nagayama, K.; Hioka, K.; Fujito, T. *Chem. Phys. Lett.* **1993**, *212*, 81−84. (f) Baldus, M.; Tomaselli, M.; Meier, B. H.; Ernst, R. R. *Chem. Phys. Lett.* **1994**, *230*, 329−336.

(3) (a) Gullion, T. *Magn. Reson. Rev.* **1997**, *17*, 83−131. (b) Gullion, T.; Schaefer, J. *J. Magn. Reson.* **1989**, *81*, 196−200. (c) Mueller, K. T.; Jarvie, T. P.; Aurentz, D. J.; Roberts, B. W. *Chem. Phys. Lett.* **1995**, *242*, 535−542.

(4) (a) Weliky, D. P.; Tycko, R. *J. Am. Chem. Soc.* **1996**, *118*, 8, 8487−8488. (b) Tycko, R.; Weliky, D. P.; Berger, A. E. *J. Chem. Phys.* **1996**, *105*, 7915−7930.

(5) (a) Tomita, Y.; O'Connor, E. J.; McDermott, A. *J. Am. Chem. Soc.* **1994**, *116*, 8766−8771. (b) Feng, X.; Lee, Y. K.; Sandstrom, D.; Eden, M.; Maisel, H.; Sebald, A.; Levitt, M. H. *Chem. Phys. Lett.* **1996**, *257*, 314−320. (c) Feng, X.; Eden, M.; Brinkmann, A.; Luthman, H.; Eriksson, L.; Graslund, A.; Antzutkin, O. N.; Levitt, M. H. *J. Am. Chem. Soc.* **1997**, *119*, 12006−12007. (d) Costa, P. R.; Gross, J. D.; Hong, M.; Griffin, R. G. *Chem. Phys. Lett.* **1997**, *280*, 95−103.

(6) (a) Jelinek, R.; Ramamoorthy, A.; Opella, S. J. *J. Am. Chem. Soc.* **1995**, *117*, 12348−12349. (b) Ketchem, R. R.; Hu, W.; Cross, T. A. *Science* **1993**, *261*, 1457−1460.

(7) Gullion, T.; Baker, D. B.; Conradi, M. S. *J. Magn. Reson.* **1990**, *89*, 479−484.

(8) (a) Tycko, R.; Smith, S. O. *J. Chem. Phys.* **1993**, *98*, 932−943. (b) Tycko, R.; Dabbagh, G. *J. Am. Chem. Soc.* **1991**, *113*, 9444−9448. (c) Vega, S.; Pines, A. *J. Chem. Phys.* **1977**, *66*, 5624−5644. (d) Wokaun, A.; Ernst, R. R. *Chem. Phys. Lett.* **1977**, *52*, 407−412.

S0002-7863(98)00191-7
Published on Web 04/30/1998

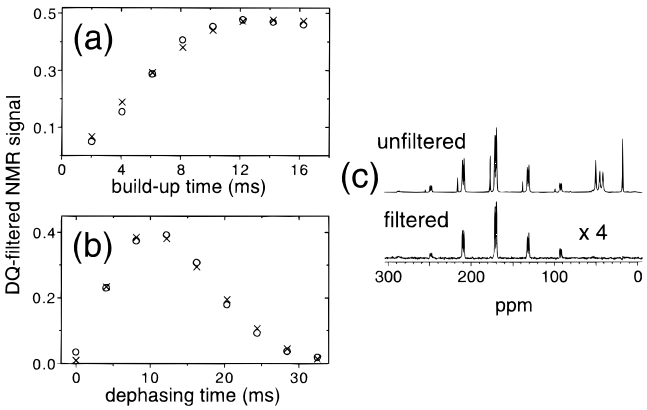

Figure 1. Experimental (circles) and calculated (crosses) constant-time dipolar evolution curves for doubly ^{13}C-labeled AGG. (a) Constant-time double-quantum build-up curve, with $L_{max} = 64$. Build-up time is $L\tau_R$. (b) Constant-time double-quantum-filtered dipolar dephasing curve, with $L_0 = 32$ and $M_{max} = 128$. Dephasing time is $2M - M_{max}$. See text for definitions of parameters and experimental conditions. Vertical scales are the calculated filtering efficiencies. (c) Solid-state MAS NMR spectra of doubly labeled AGG, with and without double-quantum filtering. Filtered spectrum corresponds to the longest build-up time in part a.

experimental data. No relaxation or damping parameters are used. The good agreement between experiments and simulations indicates the absence of large effects on the dipolar evolution curves that cannot be simulated.

The AGG sample contained 3% doubly labeled molecules, with ^{13}C labels at the carbonyls of Ala-1 and Gly-2, diluted in unlabeled AGG.[4] Experiments were performed at a ^{13}C NMR frequency of 100.8 MHz on a Chemagnetics Infinity-400 spectrometer with a Chemagnetics 6 mm MAS probe. ^{13}C π pulses in the RFDR train (one pulse per two rotor periods) were 13.7 μs and were actively synchronized with the MAS tachometer, TPPM decoupling[9] at 85 kHz was applied between the ^{13}C π pulses, and τ_R was 254 μs. Each data point resulted from 256 FIDs and was obtained by integrating carbonyl spinning sideband lines in the double-quantum-filtered MAS spectra. Figure 1c shows examples of filtered and unfiltered spectra. The experimental filtering efficiency[8] at $L\tau_R = 16.256$ ms ($T = 32.512$ ms) in Figure 1a is 0.29. Simulated curves come from numerical calculations of the quantum dynamics of the two-spin system under the full pulse sequence, including finite rf amplitudes, summed over molecular orientations. The time-dependences of dipole−dipole couplings and chemical shifts under MAS were calculated using the molecular geometry and CSA tensors described previously,[4] with dihedral angles $\phi = 83°$ and $\psi = 170°$ for Gly-2 from the AGG crystal structure.[10]

CTDQBU and CTDQFD curves obtained with RFDR depend not only on the internuclear distance but also on the orientations of the CSA tensors of the labeled sites, i.e., on both the ϕ and ψ dihedral angles between the labeled carbonyls in the case of a peptide backbone. We have recently developed rotor-synchronized two-dimensional (2D) MAS exchange spectroscopy for the determination of dihedral angles in doubly carbonyl-labeled peptides[4] by solid-state NMR. CTDQBU or CTDQFD measurements on the same samples provide complementary information. To investigate this point and the applicability of constant-time recoupling techniques to larger peptides in noncrystalline environments, a 2D MAS exchange spectrum and a CTDQFD curve were acquired for a 5 μmol sample of the 26-residue helical peptide

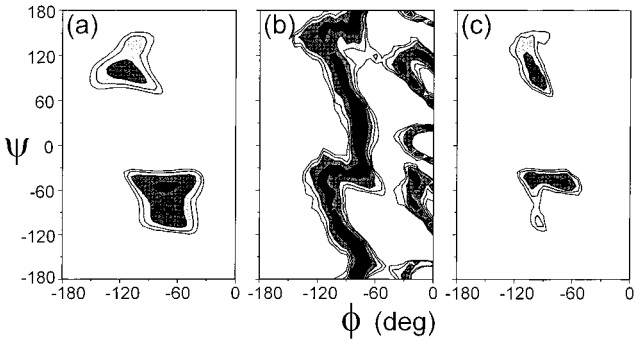

Figure 2. Analyses of 2D MAS exchange (a) and CTDQFD (b) solid state ^{13}C NMR measurements on doubly labeled melittin in frozen glycerol/water solution. The deviation Δ (defined in text) between experimental and simulated data is represented on a gray scale as a function of the ϕ and ψ dihedral angles assumed in the simulations. Part c is the sum of parts a and b. Black regions represent $\Delta \leq 10$, 2, and 13 in parts a, b, and c, respectively. Contour levels increase in units of 2.

melittin[11] in frozen glycerol/water solution (50/50 v/v) at −140 °C, with 250 mM phosphate buffer, pH 7.2, and with 10 mM $CuNa_2EDTA$ added to reduce the proton spin−lattice relaxation time to 1.5 s. Melittin was synthesized with carbonyl ^{13}C labels at Gly-3 and Ala-4. Figure 2 shows plots of the deviations Δ (see below) between experimental and simulated data as functions of the ϕ and ψ angles assumed in the simulations for the two data sets. For the 2D MAS exchange data alone, global and local minima in Δ occur at $\phi = -73°$, $\psi = -55°$ and $\phi = -112°$, $\psi = 99°$, respectively, surrounded by broad areas of relatively small Δ. For the CTDQFD data alone, ridges of minimum Δ occur. The sum of the two functions (Figure 2c) shows significantly reduced areas of minimum Δ. The global minimum in Figure 2c occurs at $\phi = -67°$, $\psi = -50°$, in good agreement with the values $\phi = -69°$, $\psi = -46°$ for Ala-4 in melittin crystals.[11]

For Figure 2, 2D MAS exchange experiments and simulations were performed as previously described.[4] The CTDQFD curve was acquired with $L_0 = 32$, $M_{max} = 80$, and $\tau_R = 254$ μs. Simulations of CTDQFD curves included rf inhomogeneity effects because of the large (240 μL) sample volume. CSA principal values were determined from spinning sideband intensities.[12] Δ is defined to be $s^2/(\sigma^2\sqrt{2(n-1)})$, with n the number of data points (20 for 2D MAS exchange, 5 for CTDQFD), s^2 the total squared deviation between experimental and simulated points, and σ^2 the mean squared uncertainty (noise plus simulation error) per point. At each ϕ,ψ pair, the scaling of the simulated data was adjusted to minimize Δ. Variations in Δ by more than approximately one unit are statistically significant. If the experimental signal-to-noise were lower, additional measurements, such as ^{15}N 2D MAS and recoupling measurements on doubly ^{15}N-labeled peptides, might be required to distinguish the global minimum in Δ from local minima in Figure 2c.

The constant-time recoupling techniques described above are relatively undemanding on rf performance and are compatible with high fields and high molecular weights. We expect these techniques to be useful in the development and testing of structural models for biomolecular and other complex systems.

Acknowledgment. Simulation programs are available on request. This work was supported by a grant from the NIH Intramural AIDS Targeted Antiviral Program.

JA980191U

(9) Bennett, A. E.; Rienstra, C. M.; Auger, M.; Lakshmi, K. V.; Griffin, R. G. *J. Chem. Phys.* **1995**, *103*, 6951−6958.
(10) Subramanian, E.; Lalitha, V. *Biopolymers* **1983**, *22*, 833−838.
(11) (a) Dempsey, C. E. *Biochim. Biophys. Acta* **1990**, *1031*, 143−161. (b) Terwilliger, T. C.; Eisenberg, D. *J. Biol. Chem.* **1982**, *257*, 6016−6022.
(12) Herzfeld, J.; Berger, A. E. *J. Chem. Phys.* **1980**, *73*, 6021−6030.